applied sciences

MDPI

Article

Rock Slope Instability Mechanism Induced by Repeated Mining in Mountain Mining Areas

Rong Luo [1,2,3], Guangyue Li [1], Lu Chen [2,*], Ling Zeng [2], Ke Pei [2] and Xiangxi Yu [2]

[1] School of Resource Environment and Safety Engineering, University of South China, Hengyang 421001, China; luorong-lr@stu.usc.edu.cn (R.L.)
[2] School of Civil Engineering, Changsha University of Science & Technology, Changsha 410110, China; peike@stu.csust.edu.cn (K.P.); 17740683572@163.com (X.Y.)
[3] Periodical Press, Changsha University of Science & Technology, Changsha 410110, China
* Correspondence: chenlu@csust.edu.cn

Abstract: When mineral resources are extracted using underground mining methods in hilly regions, landslides or slope failures can be induced frequently. In this study, slope collapse disasters in mountain mining areas were analyzed. The model test and numerical simulation of the slope impacted by repeated mining were carried out. The crack evolution and failure process were analyzed to reveal the instability mechanism. The results show that the rock mass would topple to the inside of the slope first, when the subsidence of overlying rock was induced by the mining of the upper coal seam. When repeated mining was performed in the lower coal seam, the mining induced macro-cracks that could connect with natural fissures, inducing the outward displacement of the slope. Then, the rock mass at the foot of the slope has to bear the upper load, which is also squeezed out by the collapsed rock mass, forming the potential slip zone. Finally, the instability is caused by the shear slip of the slope toe rock mass. Therefore, the instability evolution of the slope under underground repeated mining disturbance can be divided into four stages as follows: roof caving and overlaying rock subsidence, joint rock toppling, fracture penetration, and slope toe shearing and slope slipping.

Keywords: repeated mining; crack evolution; shear slip; slope instability

check for updates

Citation: Luo, R.; Li, G.; Chen, L.; Zeng, L.; Pei, K.; Yu, X. Rock Slope Instability Mechanism Induced by Repeated Mining in Mountain Mining Areas. *Appl. Sci.* **2024**, *14*, 9634. https://doi.org/10.3390/app14219634

Academic Editors: Fernando Rocha and José António Correia

Received: 26 August 2024
Revised: 2 October 2024
Accepted: 14 October 2024
Published: 22 October 2024

Copyright: © 2024 by the authors. Licensee MDPI, Basel, Switzerland. This article is an open access article distributed under the terms and conditions of the Creative Commons Attribution (CC BY) license (https://creativecommons.org/licenses/by/4.0/).

1. Introduction

In mining areas, subsidence or landslides will be caused by underground mining activities [1,2]. In particular, many mineral resources are buried in mountainous areas in the southwest of China. When the underground mining method is used to excavate the mineral resource, mountain cracking and collapse disasters of the slope can be induced easily [3,4]. Therefore, the characteristics of deformation and crack evolution are analyzed, and the influence factors of underground mining on mountain stability are investigated [5–7].

Usually, scholars focus on the investigation of the engineering conditions of the mining-induced landslide disasters [8–10]. And the model test or numerical simulation is performed to analyze the causes of instability [11–13]. Salmi et al. [14] established a discontinuous numerical model to investigate the mechanisms of the underground-mining-induced landslide that occurred in Nattai North, Australia. The results show the shear and compressive failure will be induced at the escarpment base, then the forward sliding and toppling of the rock column can be initiated. Arca et al. [15] analyzed the landslide-related factors to identify landslide susceptibility of mined disturbed areas in Kozlu, Turkey. Then, the landslide susceptibility map was established. Cui et al. [16] identified the key features and contributing factors for mining-induced landslides, and the dynamic mechanism was analyzed using geological field surveys, numerical simulation and theoretical analysis. Yang et al. [17] used the interferometric synthetic aperture radar technique and landslide and fissure spatiotemporal statistics to investigate the spreading

process of the slow subsidence caused by underground coal mining. Then, the mining impact on the occurrence of shallow loess landslides was revealed. Lai et al. [18] considered the soft–hard interlayer structure of the slope disturbed by underground mining, and centrifuge model tests and 3D discrete element mode were performed to investigate the Madaling landslide. The displacement of the deep rock mass is proposed to serve as the early-warning criterion for mining landslides. Liu et al. [19] designed a two-stage monitoring system to identify the potential landslide area and record multiple real-time data regarding an impending landslide. Zhong et al. [20] investigated the formation mechanism of a landslide occurring in coal-mining subsidence area at the Tanshan Coal Mine in Ningxia. The stress and deformation characteristic during the failure process were discussed, which was divided into four stages: slope creep, slope deformation, landslide movement and landslide accumulation.

The previous studies show that the collapse of slopes located in hilly regions is easily induced by underground mining. Researchers focus on the description of the collapse phenomenon, offering critical insight into the mechanism of the landslide [21,22]. However, the key factor of repeated mining has inadvertently been ignored. Some mining landslides revealed that multiple coal seams were mined in the collapse area [23]. To reveal the instability mechanism induced by the repeated mining, the mined induced collapse disasters that occurred in the Pusa Village were analyzed. The model test and numerical simulation of slope disturbed by underground repeated mining were established. The failure process was analyzed to investigate the characteristics of deformation, crack evolution and sliding.

2. The Background of the Landslide

2.1. Overview of the Landslide

Abundant coal resources are buried in the Laoyingyan Mountain, Pusa Village, Zhangjiawan Town, Nayong County, Guizhou Province, which have been extracted using underground mining methods for many years, forming a complex goaf. As shown in Figure 1, due to the combined effect of the primary structural plane, mining and weathering, deep cracks occurred on the mountaintop. The stability of the mountain slope decreases significantly. At about 10:40 PM on 28 August 2017, a large slope collapse disaster occurred. The length and width of the collapse were about 840 m and 410 m, respectively. The volume was about 6×10^5 m^3. The surrounding woodland and farmland were destroyed. Some houses located in the lower part of the village were buried, resulting in a total of 35 deaths [8].

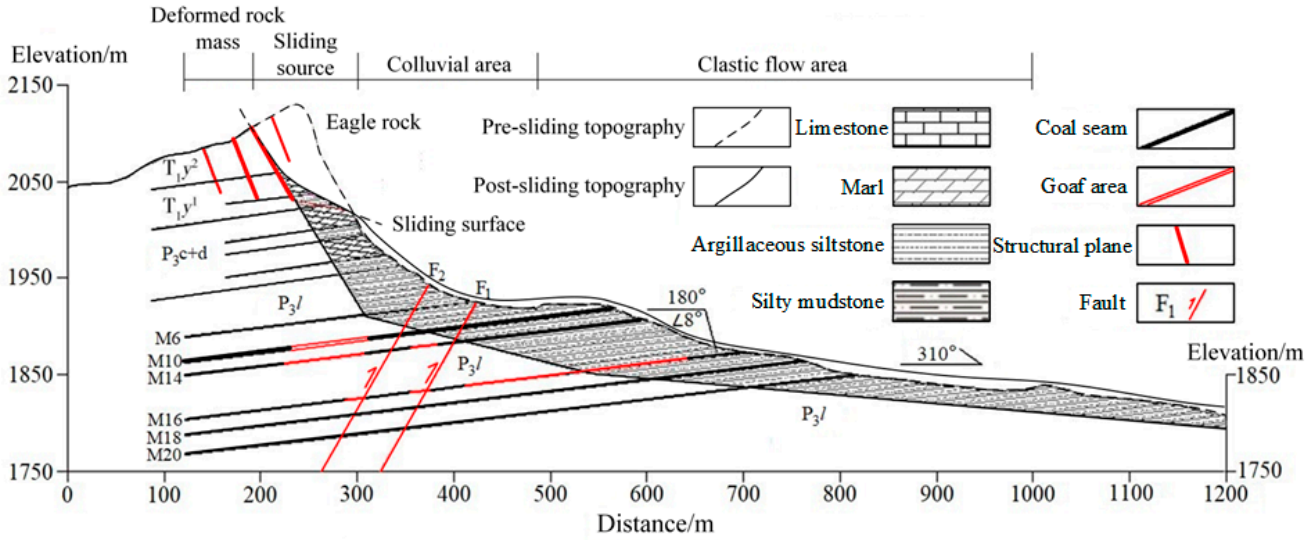


Figure 1. Geological profile of the collapse area.

2.2. Engineering Geological Condition

2.2.1. Stratigraphic and Lithologic Structure

The strata in the collapse area include the following: clay and sandy clay in the Quaternary; in the Triassic Yelang Formation (T1y), the upper part is gray-brown medium-thick limestone with marl, and the lower part is gray sandy mudstone with siltstone; in the Triassic Changxing–Dalong Formation (P_2c + d), the upper part is marl with shale, and the lower part is gray medium-thick-layered and thin-layered limestone; the Permian Longtan Formation (P_3l), which is the coal measure strata, includes gray-green-deep gray silty mudstone, gray-deep gray argillaceous siltstone and coal seam. Some rock mechanics tests are performed; the mechanical parameters of rock are listed in Table 1.

Table 1. Mechanical properties of rock.

Lithology	Density/(g/cm^3)	Strength/MPa	Young's Modulus/GPa
Limestone	2.67~2.72	57.6~85.6	9.51~36.7
Marl	2.62~2.69	43.3~64	6.47~30
Silty mudstone	2.54~2.65	33.9~56.2	5.18~14
Coal	1.3~1.4	4.65~20	0.76~3.5
Muddy siltstone	2.58~2.66	22.4~47.5	2.15~12

2.2.2. Geological Structure

The strata in the collapse region has a monoclinic structure. The dip direction is 138–187°, and the dip angle is 7–10°. The occurrence of a coal seam is consistent with that of the strata. Affected by lithology composition, the limestone and marl located at the upper of slope are relatively hard in strength, and the lower mudstone and siltstone are low, forming the upper hard and lower soft structure. Therefore, the slope rock mass is characterized as soft and hard interbedded. Furthermore, the mining area is disturbed by three faults, F1, F2 and F3 [24]. F1 is a normal fault, which has an NE dip direction with an angle of 155–167° and a dip angle of 63–70°. F2 is a reverse fault, dipping to southeast, with an angle of 70–75°. F3 is a normal fault, dipping to the northeast, with an angle of 75–80°. Among them, F1 and F2 are developed in the middle and front of the slope at the lower part of the cliff in the collapse area, cutting the coal seam in the mining area. F3 is located about 500 m to the east of the collapse area. The collapse area cannot be affected by those faults. However, the rock mass structure at the top of the eagle rock is broken, and the joint fissures are developed, forming the four groups of structural planes. The depth is 50–80 m, and the width is 2–3 m. Those are considered as the seepage channel. The surface water can flow into the underground goaf. The strength of the rock will deteriorate, impacting the stability of the slope.

2.3. The Underground Mine

Six minable coal seams are buried under slope, which are named M6, M10, M14, M16, M18 and M20, from top to bottom. The dip angle of the coal seams is between 7° and 12°. M10, M14 and M16 are mainly excavated in the collapse area, and the average thickness of the coal seams is 2.12, 1.23 and 1.48 m, respectively. The roof and floor of the coal seams are argillaceous siltstone. The mining area under the mountain is about 0.96 km^2. According to the characteristics of coal seams, the longwall retreating mining method is used. Before 2010, M16 was mainly excavated. The goaf of M16 was located at the front end of the slope, which has little effect on the deformation of the slope. The M10 and M14 coal seams were mainly excavated from 2011 to the time before the occurrence of collapse. The goafs of the M10 and M14 coal seams were located directly below the slope. When the M10 and M14 coal seams were excavated, a macro-fracture was caused at the top of the mountain. Then, the mountain began to deform violently.

3. The Model Test of the Collapse

3.1. Model Design

A frame and a non-contact displacement monitoring system are used in the model test. The maximum dimension of the model is 1300 mm × 1000 mm × 150 mm. The monitoring system is composed of an image acquisition and analysis system. A charge-coupled device camera was used to record the digital images of the model. And the deformation characteristic is analyzed using the digital speckle correlation method. By tracking the same pixels occurring in the digital images recorded before and after deformation of the model, the displacement and deformation of the monitored area can be calculated [25]. In this study, the charge-coupled device camera (CCD) and the image storage device were used. The maximum resolution and speed of the CCD is 2456 pixels × 2058 pixels and 75 M/s, respectively. During the mining process, a resolution of 1280 pixels × 960 pixels and a 5 Hz acquisition rate were set to capture the deformation digital images.

As shown in Figure 2, considering the similarity ratio and experimental feasibility, the simplified similarity model was established based on the engineering and mining conditions of the Laoyingyan Mountain. The mechanical and geometrical similarity ratios of the similarity model were designed as follows: C_L = 1:300, C_S = 1:330 and C_ρ = 1:1.1 ($C_{L,S}$ and C_ρ are the similarity constant for geometry, stress and density, respectively). Details of the material similarity for the model test and similarity criteria can be found in our previous publications [26,27]. The mechanical parameters of stratum are shown in Table 2. Two mineable coal seams were designed. The length and height mined of the upper coal seam were 60 cm and 2.5 cm, respectively. The length mined of the lower coal seam was also 60 cm, and the mining height was 1.5 cm. A speckled pattern was sprayed on surface of the model. The coal mining was carried out from the inside of the slope to the free face continually. In this study, a positive value indicates that the horizontal displacement of the slope is towards the free surface, and the vertical displacement is downward. The six characteristic states of the model are analyzed. Both the upper and lower coal seams are divided into three stages. The sequence is S1 → S2 → S3 → X1 → X2 → X3, and the interval length was 20 cm.

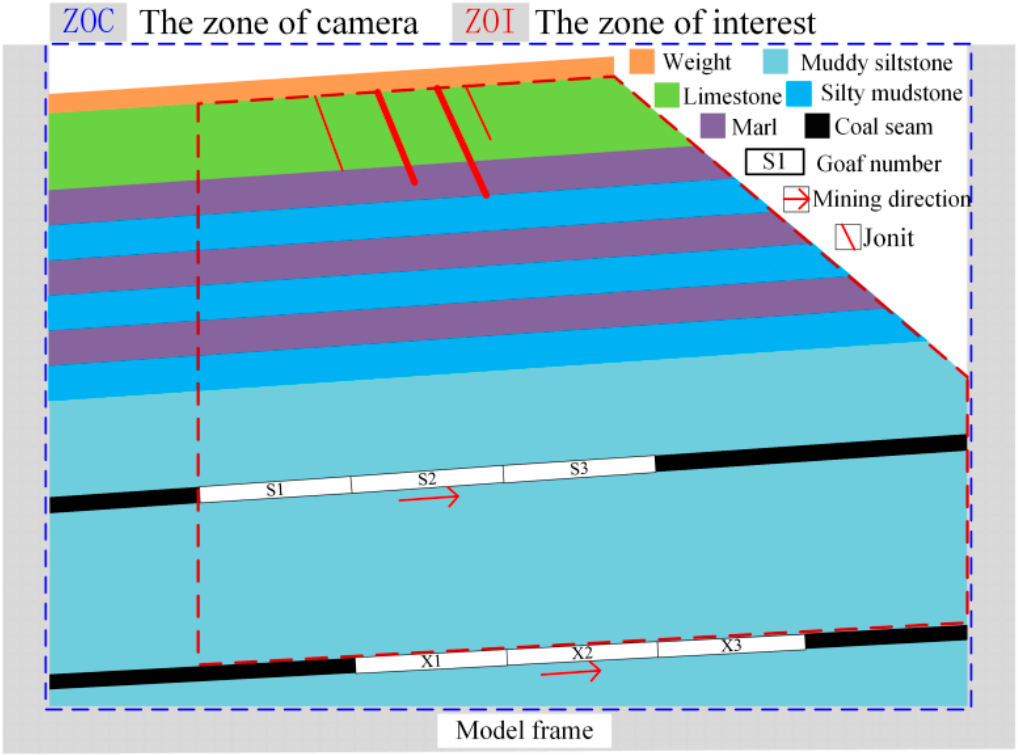


Figure 2. The similarity model.

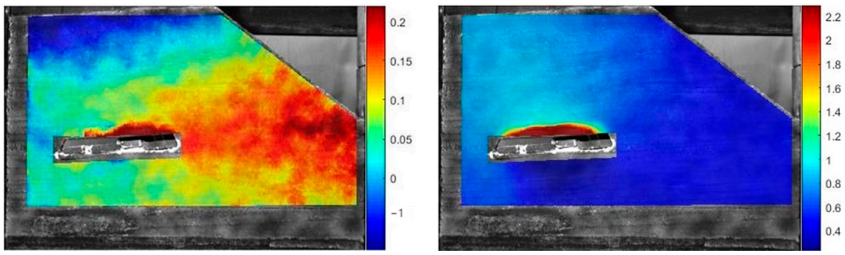
Table 2. Mixture ratio and mechanical parameters of similarity material.

Lithology	Mixture Composition					Strength (MPa)	Young's Modulus (MPa)
	Sand (kg)	Barite Powder (kg)	$CaCO_3$ (kg)	Gypsum (kg)	Water (kg)		
Limestone	22.91	9.82	0.16	1.47	3.82	0.227	29.6
Marl	11.50	4.93	0.33	0.49	1.92	0.165	20
Silty mudstone	12.81	3.20	0.40	0.40	1.33	0.157	15.4
Muddy siltstone	54.36	6.04	1.81	1.21	3.02	0.115	6.6
Coal seam	2.82	0.31	3.14	0.00	1.15	0.014	2.4

3.2. The Displacement Induced by the Mining

3.2.1. The Displacement Induced by the Mining of the Upper Coal Seam

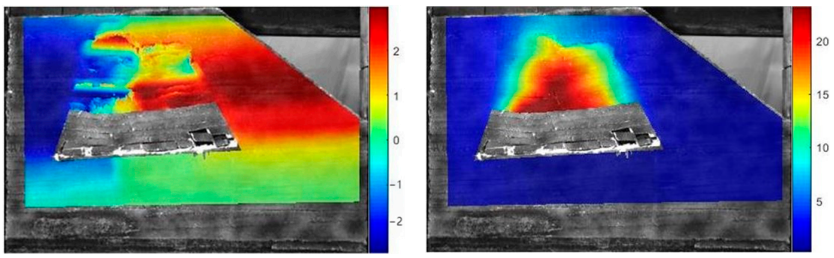
The displacement of the model induced by the mining of S1 and S2 in the upper coal seam is shown in Figure 3. When S1 and S1 were mined, a slight displacement was caused. The horizontal displacement mainly occurred in the roof caving zone and slope toe. The vertical displacement mainly occurred at the middle of the roof of the working face, and the maximum value was 5.5 mm, which indicates that the mining of S1 and S2 had a great influence on the deformation of the immediate roof and had little influence on the slope.



(**a**) (**b**)

Figure 3. The displacement induced by the mining of S1 and S2. (**a**) Horizontal displacement; (**b**) vertical displacement.

The displacement of the model induced by the mining of S3 is shown in Figure 4. The significant displacement was caused in the upper rock mass of the slope. The boundary of mining-induced fracture could be clearly identified. The vertical displacement mainly occurred above the goaf. The closer to the goaf, the greater the displacement. The settlement value of the model top was between 5 mm and 7 mm, which indicates that the mining influence had been transmitted from the roof to the top of the model through the overburden rock. However, the vertical displacement of the slope surface was still small. The horizontal displacement mainly occurred in the upper part of the goaf and the slope surface. The deformation boundary was generated at the middle of the goaf, and the displacement direction was different in that area. This indicates that the roof caved into the goaf, and the collapsed rock mass squeezed the slope, which moved towards the free surface. Therefore, the stability of the mountain was significantly reduced.



(**a**) (**b**)

Figure 4. The displacement induced by the mining of S3. (**a**) Horizontal displacement; (**b**) vertical displacement.

3.2.2. The Displacement Induced by the Mining of the Lower Coal Seam

The displacement of the model induced by the mining of X1 is shown in Figure 5. As the model in this stage is very different from the initial state, the initial state of mining of the lower coal seam is taken as the reference frame in the digital speckle analysis. When X1 was mined, the displacement of the roof of the lower coal seam was relatively small. However, the obvious stratification was caused in the overlying strata. The impact zone was larger than the mined range. This indicates that the smaller subsidence of the roof of the lower coal seam may lead to a larger displacement of the upper rock layer.

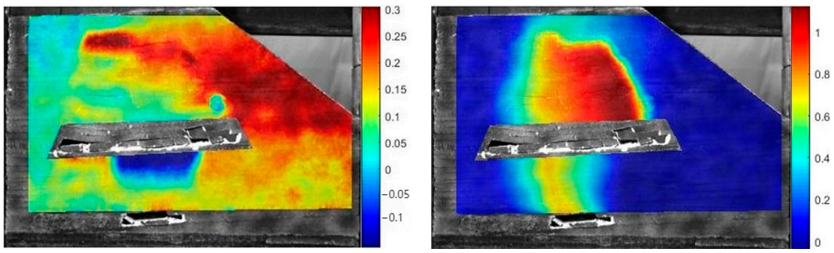


Figure 5. The displacement induced by the mining of X1. (**a**) Horizontal displacement; (**b**) vertical displacement.

The displacement of the model induced by the mining of X2 is shown in Figure 6. Affected by the large-area caving of the lower coal seam roof, the deformation of the slope increased obviously, which resulted from the mining of X2. In the horizontal direction, significant displacement occurred at the position on the right side of the upper roof and the middle of the lower coal seam, and the maximum value was 3.7 mm. This indicates that the broken rock layer was continuously toppled outward with the excavation of the lower coal seam, and the slope surface rock mass was squeezed at the same time. In the vertical direction, significant displacement occurred at the position on the middle of the roof of the lower coal seam. Obvious displacement was also caused at the position on the right side of the upper roof. At this time, the influence of underground excavation on the top of the slope was slight, and the settlement value was less than 2 mm.

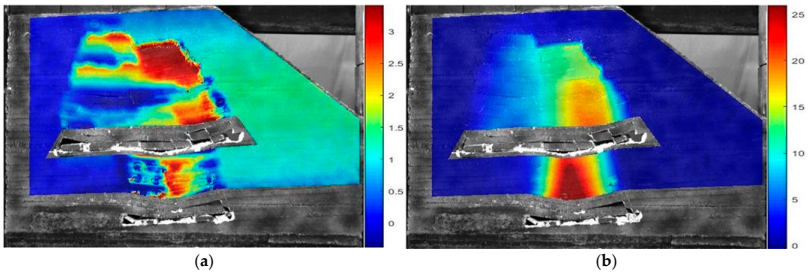


Figure 6. The displacement induced by the mining of X2. (**a**) Horizontal displacement; (**b**) vertical displacement.

The displacement of the model induced by the mining of X3 is shown in Figure 7. When the lower coal seam was completely excavated, part of the slope displacement value of the model failed to display, as the rock had been seriously broken, and the speckle pattern on the surface was damaged. Hence, the displacement cannot be identified using the digital speckle correlation method. It can be seen from the existing data that the significant horizontal displacement was caused in the middle of the broken rock mass, and the maximum value reached 19.8 mm. The slope toppled to the free surface, and the potential sliding surface was penetrated. Significant vertical displacement was also induced at the right side of the broken rock mass. The slope had been in a critical state. Further underground mining or other disturbances may induce landslides.

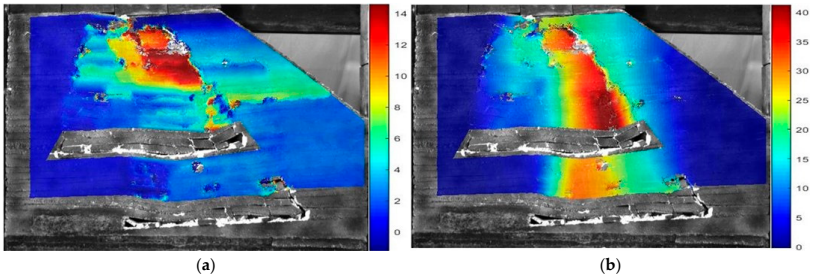


Figure 7. The displacement induced by the mining of X3. (**a**) Horizontal displacement; (**b**) vertical displacement.

4. Numerical Simulation Analysis of the Collapse

4.1. Scheme of Numerical Simulation

4.1.1. The Numerical Model

Based on the engineering geological condition, the repeated-mining-disturbed numerical model was established using the PFC 2D (Particle Flow Code 5.0) discrete element software, as shown in Figure 8. The complete process of crack initiation and propagation induced by the excavation disturbance can be simulated [28,29]. The length of the model was 500 m, and the width was 345 m. The geological characteristics of the slope were designed basically. Two minable coal seams buried under the slope were established. The thickness of the upper and lower coal seams was 7 m and 4 m, respectively. The limestone, marl silty mudstone and muddy siltstones were designed as the overburden. The dip angle of the rock stratum in the numerical model was 10°. Four joint fissures were set at the top of the model to simulate the structural plane of the mountain prototype. The fissure depth changed from 50 m to 80 m, and the dip angle was about 70°. The horizontal displacement of the left and right boundaries of the model was limited; the vertical displacement of model at the potion of the bottom boundary was also limited. The parallel bond model was used for simulating the mechanical behavior of the coal and rock mass. If the tensile-strength limit is exceeded, then the bond in tension is broken. If the bond has not broken in tension, then the shear-strength limit is enforced, and the stiffness will reduce with the breaking of the bond. Hence, this model is considered as a suitable bond model for the rock materials [30]. The parameters in the numerical model were listed in Table 3, which were determined by referring to the previous research and parameter calibration test [24,31]. In the numerical model, the unconfined compression strength of limestone, marl, silty mudstone, coal and muddy siltstone is about 69 MPa, 54 MPa, 51 MPa, 4.7 MPa and 38 MPa, respectively, according to the parameters listed in Table 3.

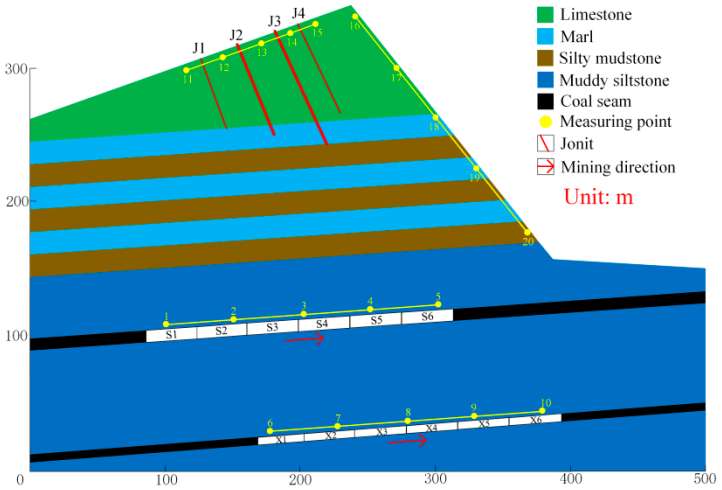


Figure 8. The numerical model.

Table 3. The parameters in the numerical model.

Parameter	Limestone	Marl	Silty Mudstone	Coal Seam	Muddy Siltstone
Porosity (%)	0.1	0.1	0.1	0.1	0.1
Particle density (kg/m^3)	2700	2650	2600	1350	2560
Effective modulus/GPa	10	8	7	1.84	5.6
Bond normal-to-shear stiffness Ratio ($\bar{k}^*$)	1	1	1	1	1
Bond effective modulus/GPa	10	7	5	1.84	4.6
Bond tensile strength/MPa	15	12.5	10.2	3.15	8
Bond cohesion/MPa	25	18.1	15.4	5.53	14.45
Bond friction angle/°	38	35	33.8	18	30.1

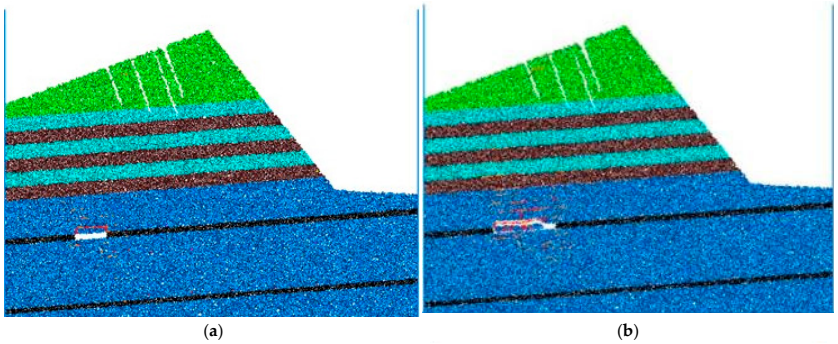
4.1.2. Excavation and Monitoring

The upper and lower coal seams were excavated, respectively. Each coal seam was mined from the inside of the slope to the outside of the slope. The length of the work face was 240 m. In order to investigate the deformation response law of the layered rock slope under excavation disturbance, a total of 20 monitoring points were laid out as shown in Figure 8. On the roof of the lower and upper coal seams and the top and surface of slope were set five monitoring points, respectively. When the coal seam was mined for 40 m, the crack and displacement were recorded and analyzed. The sequence was marked as S1 → S2 → S3 → S4 → S5 → S6 → X1 → X2 → X3 → X4 → X5 → X6.

4.2. Analysis of the Failure Process

4.2.1. The Mining of the Upper Coal Seam

Figure 9 exhibits the fracture evolution of the slope during the excavation of the upper coal seam. When the upper coal seam was mined for 40 m, the separation was caused in the immediate roof. Due to the large span of the working face, the immediate roof first collapsed after the mining length of 80 m. Some separations were caused in the overlying strata. After the mining of S3, the overlying strata above the working face collapsed as an inverted trapezoid, and some separation fissures were caused between the marl and mudstone. At this time, the rock mass cut by the deep structural plane at the top of the slope toppled towards the inside slope, resulting in the closure of J3. When S4 was mined, the caving area continued to increase, and the mining-induced cracks on the left boundary also expanded upward. Tensile cracks appeared at the bottom of the rock bridge on the top of the slope, and J2 gradually closed. When S5 was mined, a large displacement had been caused in the overlying strata, and the marl and mudstone above the working face collapsed completely. The mining-induced cracks had been transmitted upward to the surface, and the joint rock toppled to the trailing edge of the mountain. Some cracks were induced at the foot of the slope. After the mining of S6, the range of the fracture zone above the goaf was further expanded. The slope stability was significantly reduced due to the oblique tension crack in the middle of the slope.



(**a**) (**b**)

Figure 9. *Cont.*

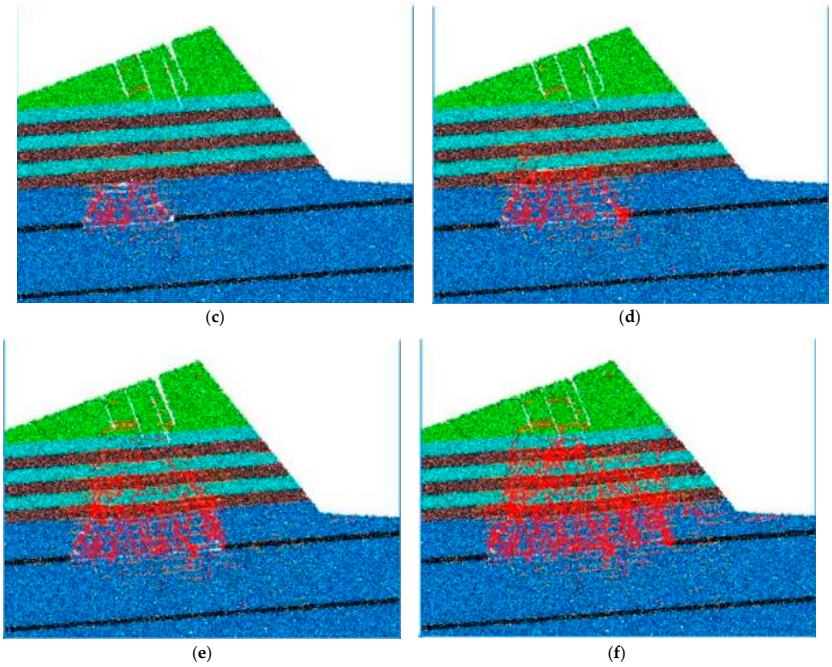


Figure 9. The fracture evolution during the mining process of the upper coal seam. (**a**) S1; (**b**) S2; (**c**) S3; (**d**) S4; (**e**) S5; (**f**) S6.

4.2.2. The Mining of the Lower Coal Seam

Figure 10 exhibits the fracture evolution of the slope during the excavation of the lower coal seam. After the excavation of X1, the separation was caused in the roof. However, the mining has a slight effect on the roof of the upper coal seam. When X2 was mined, the immediate roof collapsed, and the main roof subsided. The mining fracture zone expanded upward, resulting in a small settlement of the mining zone of the upper coal seam. After the mining of X3, a large-area roof of the working face caved, and the fracture zone had expanded to the floor of the upper coal seam. After the mining of X4, the overlying strata of the working face sank, which led to obvious subsidence in the upper mining zone, and the joint rock on the top continued to move into the slope. At this time, the surface rock mass at the foot of the slope was uplifted. After the mining of X5, the influence range of the goaf was further expanded, and the rock mass at the bottom of J1 was cracked. Furthermore, the rock mass at the upper part of the slope had a tendency to slide downward. The potential sliding surface was formed. However, part of roof at the right boundary of the goaf had not collapsed completely, which could support the overlying rock temporarily. After the mining of X6, the rock mass above the working face collapsed completely, the rock mass at the inside of the slope was broken extremely and step-shaped subsidence pits were caused on the joint surface of the slope top. The rock mass at the foot of the slope was squeezed out, and the slope body slipped slightly in the direction of the free surface; the potential sliding surface had essentially penetrated.

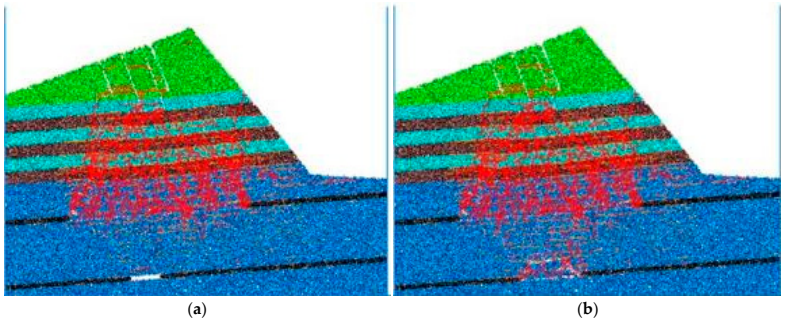


Figure 10. *Cont.*

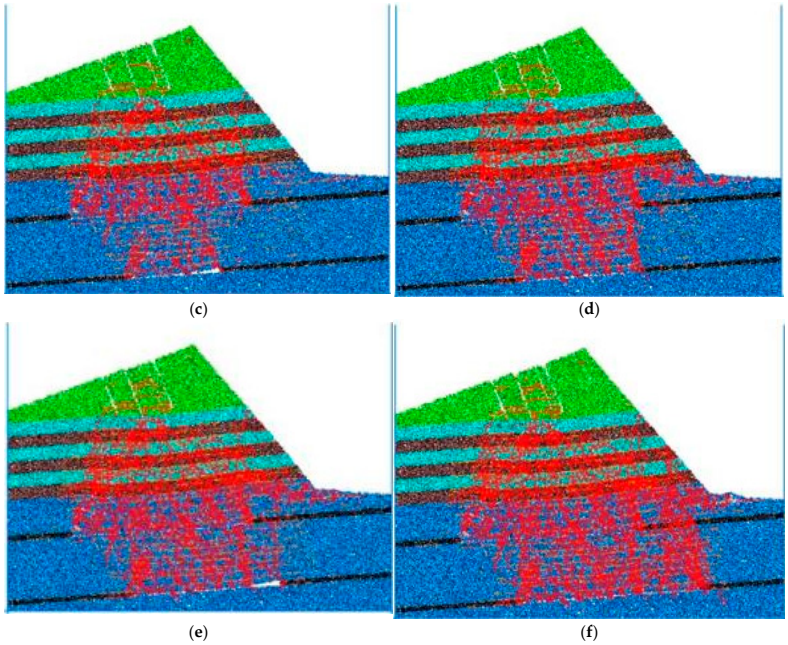


Figure 10. The fracture evolution during the mining process of the lower coal seam. (**a**) X1; (**b**) X2; (**c**) X3; (**d**) X4; (**e**) X5; (**f**) X6.

4.3. Slope Deformation Induced by Mining

4.3.1. The Displacement Characteristic of the Slope

The displacement characteristic of the slope during the mining process of the upper coal seam is shown in Figure 11. After the mining of S3, the overlying rock of the working face caved, and the settlement was characterized as an arch shape. The rock above J3 was toppled into the slope. After the mining of S6, a huge arch-shaped settlement area was formed in the middle of the slope. At this time, the vault settlement area had expanded upward to the bottom of the joint rock, resulting in the rock at the top of the slope dumping into the slope. When X3 was mined, the bending deformation was induced in overlying rock above the working face. The collapsed rock mass induced by the upper coal seam mining area continued to sink. At this time, the joint rock continued to pour into the slope. The strata of the slope above the goaf were borne by the rock mass at the toe of the slope. After the mining of X6, the overlying strata above the lower coal seam completely collapsed, and the impacted area had expanded to the foot of the slope. The support capacity of the slope toe was weakened, which failed to bear the load of the upper rock mass. The rock mass at the foot of the slope was cut off, forming a potential slip surface, and the upper rock mass began to slip towards the free surface.

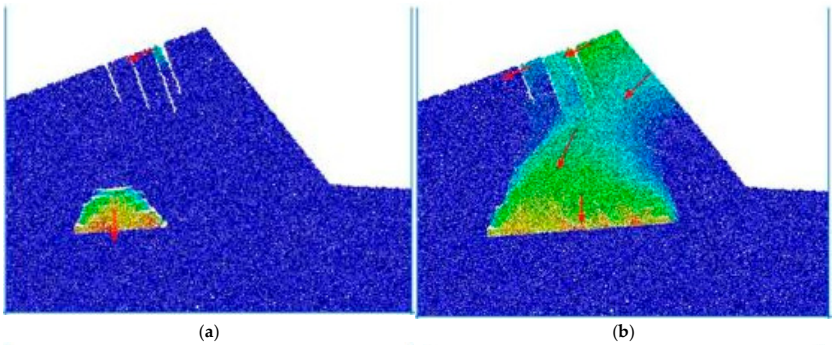


Figure 11. *Cont.*

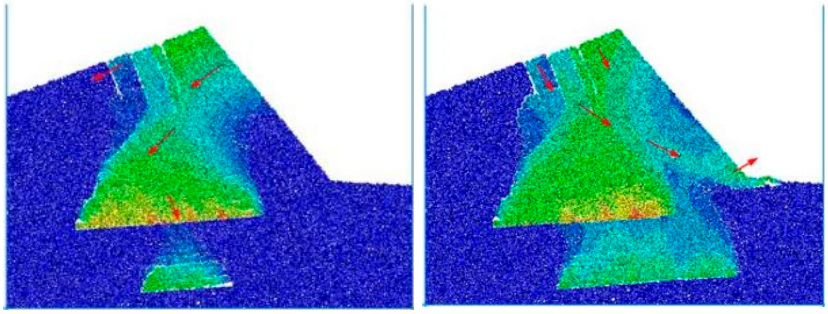


Figure 11. The displacement characteristic of the slope during the mining process. (**a**) S3; (**b**) S6; (**c**) X3; (**d**) X6.

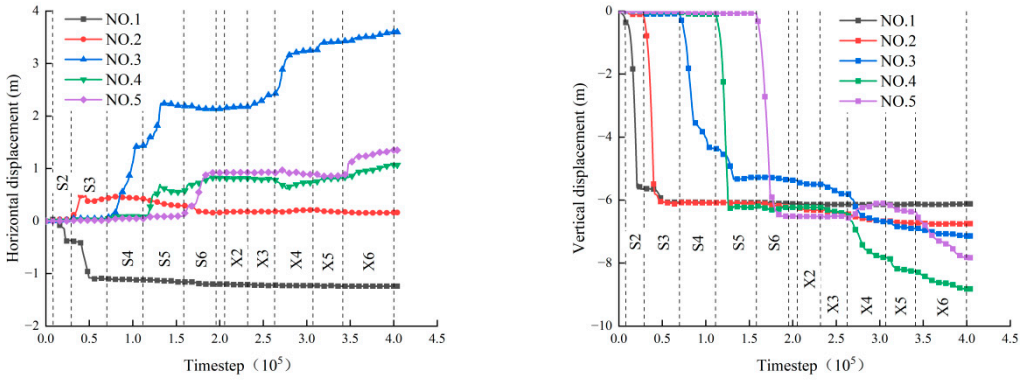
4.3.2. The Displacement Characteristic of the Measuring Point

The displacement of measuring points in the roof of the upper coal seam is shown in Figure 12. When the upper coal seam was mined, the measuring points moved rapidly, as the immediate roof collapsed with mining. Then, the displacement stopped increasing, resulting from the end of the roof collapse. With the excavation of the lower coal seam, the displacement of the measuring points in the lower coal seam roof increased accordingly, as shown in Figure 13. When X4 was mined, significant displacement was induced again in the measuring points No. 6–No. 10. This indicates that the immediate roof collapsed gradually, and the deformation of the upper coal seam floor was then activated, causing the secondary subsidence of collapsed strata of the upper coal seam. Hence, the displacement of the measuring points started to increase. During the mining process of the lower coal seam, No. 6 and No. 7 first moved to the outside of the slope, and a sudden turning change was then caused. This may be caused by the bending deformation and collapse of the immediate and main roof.

The displacement of the measuring points at the top of the slope is shown in Figure 14. The horizontal displacement of the No. 11 measuring point was different from that of the other measuring points. When the upper coal seam was mined, the displacement value of the No. 22–No. 15 measuring points reduced, indicating the rock moved to the inside of the slope. When the influence range of the mined-out area had extended to the rock above J2, the displacement of No. 14 at the position above J2 increased rapidly, indicating the rock began to fall towards the slope. During the mining of S5, the displacement of No. 12 and No. 13 increased and then decreased. This indicates the joint rock was broken first, due the subsidence of the strata, which toppled to the inside. With the increase in the subsidence range, the measured points also moved to the outside of the slope. When the lower coal seam was mined, with the increase in the excavation distance, the displacement of most measuring points gradually moved to the outside. However, the displacement of the No. 15 measuring point continued to increase until X5 was mined. This indicates the rock mass above J4 also moved to the outside. Then, the rate of change increased suddenly, indicating the slope had begun to accelerate to slip at this time. During the mining process, the displacement of No. 11 located on the left side of J1 was lower than that of the other measuring points laid out at the top of the slope. This indicates that, under the disturbance of mining, differential deformation was induced on both sides of the joint rock mass at the top of the slope. The broken joint rock would lose its support, toppling into the slope. Then, the collapsed rock had a tendency to slip outward, which contributed to form the potential sliding of the slope.

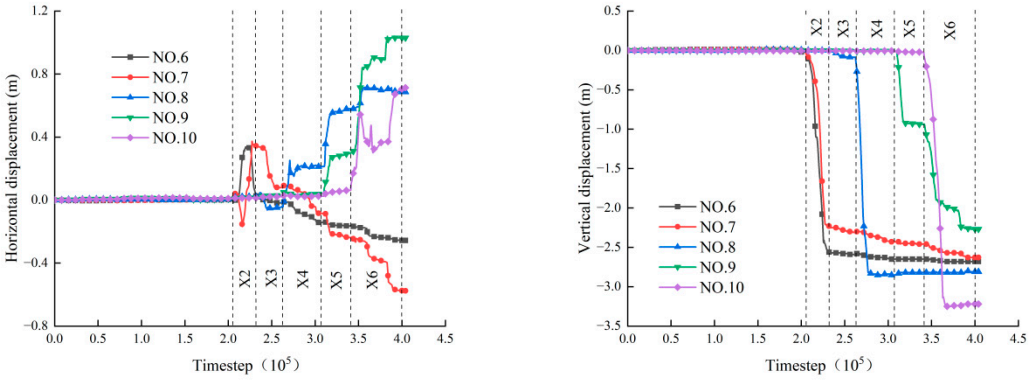
The displacement of the measuring points at the surface of the slope is shown in Figure 15. When the upper coal seam was mined, bending deformation of the overburden rock was induced. Hence, the No. 16–18 measuring points mainly moved towards the inside of the slope first, while a tiny upward movement was induced in the No. 19 and No. 20 measuring points. During the mining process of the lower coal seam, as the cracks were induced at the foot of the slope, the No. 16–18 measuring points started to move towards

the outside of the slope. The horizontal displacement value of the No. 20 measuring point was much larger than the vertical displacement value, indicating that the slope toe was mainly squeezed out in the direction of the free surface.



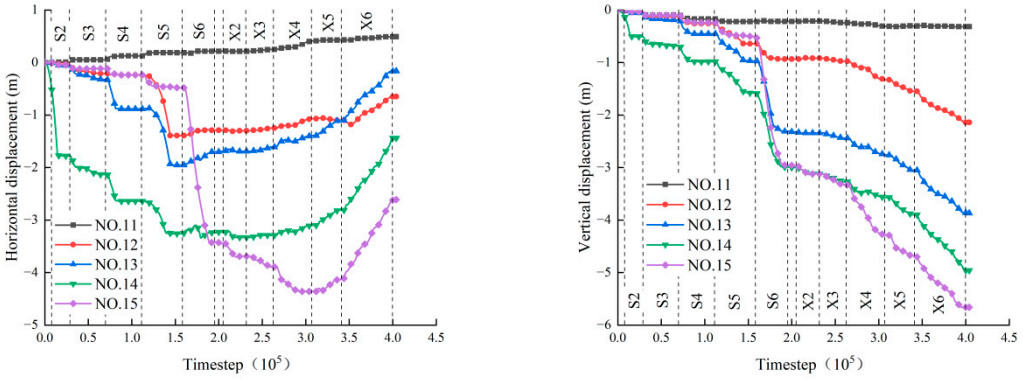
(**a**) (**b**)

Figure 12. The displacement of measuring points in the roof of the upper coal seam. (**a**) Horizontal displacement; (**b**) vertical displacement.



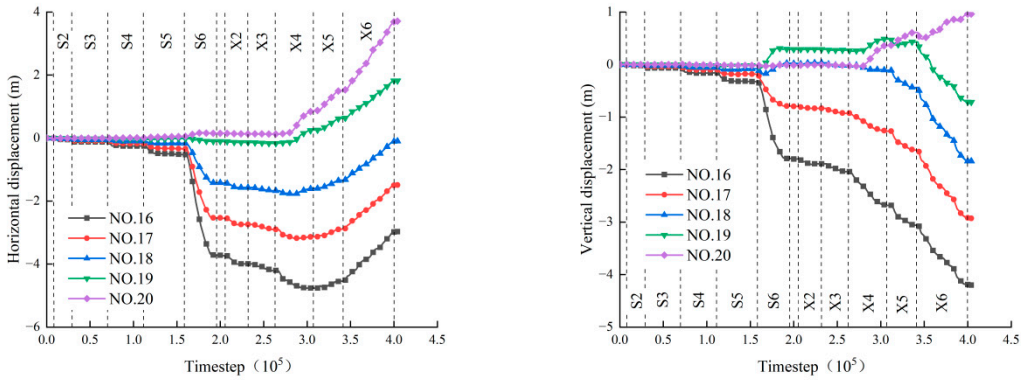
(**a**) (**b**)

Figure 13. The displacement of measuring points in the lower coal seam roof. (**a**) Horizontal displacement; (**b**) vertical displacement.



(**a**) (**b**)

Figure 14. The displacement of measuring points at the top of the slope. (**a**) Horizontal displacement; (**b**) vertical displacement.



(**a**) (**b**)

Figure 15. The displacement of measuring points at the surface of the slope. (**a**) Horizontal displacement; (**b**) vertical displacement.

5. Slope Instability Slip Mechanism

As shown in Figure 16, combined with the results of model test and numerical simulation analysis, the instability evolution of the slope under underground repeated mining disturbance can be divided into four stages as follows: roof caving and overlaying rock subsidence, joint rock toppling, fracture penetration, and slope toe shearing and slope slipping. The failure mechanism of slope instability can be summarized as strata collapse–joint rock toppling–shear slip. The main reasons for the instability and slip of the slope will be divided into geological factors and non-geological factors. In the collapse area, the geological factors were characterized as the typical upper hard and lower soft, upper steep and lower gentle slope. During the long period of weathering and karstification, many deep and large joints are developed at the top of the slope, and the stability of the mountain will be impacted. Non-geological factors include external disturbances such as underground excavation, rainfall and earthquakes.

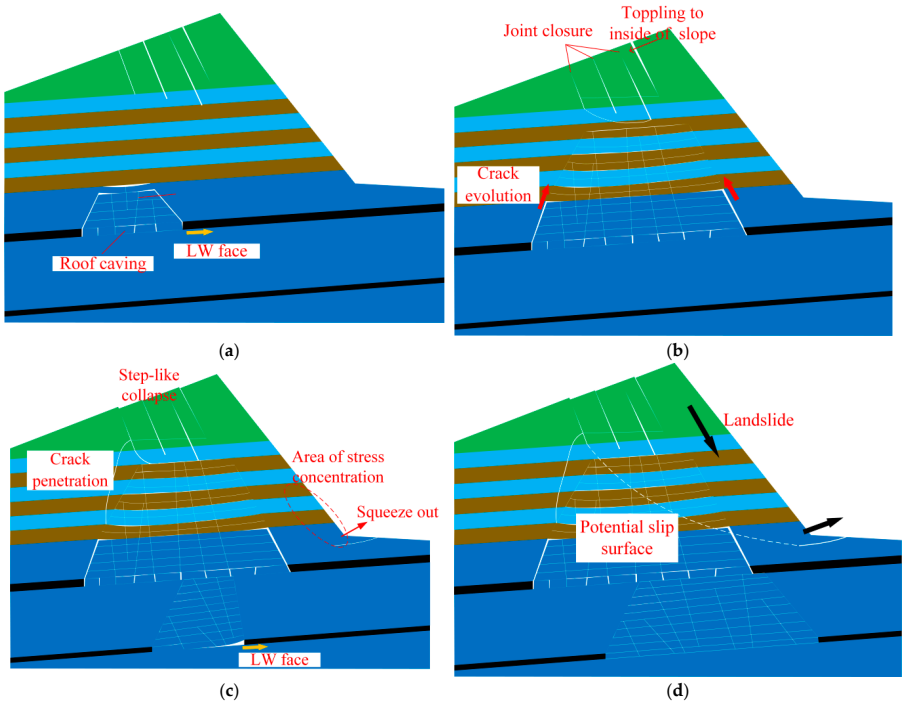


Figure 16. Slope instability process. (**a**) Roof caving and overlaying rock subsidence; (**b**) joint rock toppling; (**c**) crack penetration; (**d**) slope toe shearing and slope slipping.

When the underground resource is mined repeatedly, the joint rock can be broken during the mining process of the upper coal seam. The deep and large fissures of the slope continuously developed, and the mining-induced cracks will connect with natural fissures. In addition, water can penetrate into the slope along the cracks, and the conditions of the slope are further disturbed and deteriorated. Finally, the potential slip surface will be formed. When the rock mass at the foot of the slope is sheared and squeezed out, the rock of the slope loses support, forming a potential sliding zone and eventually leading to the slip of the slope.

6. Conclusions

In this study, the landslide disaster in Pusa Village is taken as the engineering background; the model test and numerical simulation were performed to investigate crack propagation and the mechanism of a landslide induced by repeated mining. The following specific conclusions can be made:

(1) During the repeated mining process, the joint rock mass at the top of the mountain will be broken by the mining of the upper coal seam. The rock mass topples to the inside of slope first. Then, the outward displacement of the slope will be caused by the mining of the lower coal seam. The potential slip zone will be formed.
(2) The immediate rock caving and strata subsidence will be caused by the mining. When the mining-induced crack connects with natural fissures, the rock mass at the foot of the slope has to support the overlying rock mass, which is also squeezed by the collapsed rock mass. Hence, shear cracking can be caused at the foot of the slope.
(3) The instability evolution of the slope under underground repeated mining disturbance can be divided into four stages as follows: roof caving and overlaying rock subsidence, joint rock toppling, fracture penetration, and slope toe shearing and slope slipping.

Author Contributions: Conceptualization, R.L.; formal analysis, G.L.; funding acquisition, L.C.; investigation, R.L.; methodology, L.Z.; project administration, L.C. and R.L.; testing, X.Y. and R.L.; software, X.Y. and K.P.; writing—original draft, R.L. and G.L.; validation, L.C. and L.Z. All authors have read and agreed to the published version of the manuscript.

Funding: This research is funded by the National Natural Science Foundation of China (52004036) and the Key Laboratory of Advanced Engineering Materials and Structural Mechanical Behavior and Intelligent Control for Universities in Hunan Province (19ka01).

Institutional Review Board Statement: Not applicable.

Informed Consent Statement: Not applicable.

Data Availability Statement: The data and materials are contained within the article.

Acknowledgments: We would like to acknowledge the editors and reviewers for their invaluable comments.

Conflicts of Interest: The authors declare no conflicts of interest.

References

1. Takashi, S.; Hiroshi, T.; Hideki, S.; Jiro, O.; Akihiro, H.; Kikuo, M. Surface subsidence due to underground mining operation under weak geological condition in Indonesia. *J. Rock Mech. Geotech. Eng.* **2015**, *7*, 337–344.
2. Chi, S.; Yu, X.; Wang, L. Method of predicting dynamic deformation of mining areas based on synthetic aperture radar I interferometry (InSAR) time series Boltzmann function. *Appl. Sci.* **2024**, *14*, 7917. [CrossRef]
3. Chen, L.; Yu, X.; Luo, R.; Zeng, L.; Cao, H. High steep rock slope instability mechanism induced by the pillar deterioration in the mountain mining area. *Mathematics* **2023**, *11*, 1889. [CrossRef]
4. Zhong, Z.; Xu, Y.; Wang, N.; Liu, X.; Gao, G. Environmental characteristics and unified failure mode classification system for mining landslides in the Karst mountainous areas of southwestern China. *Carbonates Evaporites* **2023**, *38*, 2. [CrossRef]
5. Qiu, Y.; Shang, Y. Analysis of progressive failure mechanism of loose slope under seismic load. *J. China Foreign Highw.* **2022**, *42*, 15–21.
6. Fernández, P.; Granda, G.; Krzemień, A.; Cortés, S.; Valverde, G. Subsidence versus natural landslides when dealing with property damage liabilities in underground coal mines. *Int. J. Rock Mech. Min. Sci.* **2020**, *126*, 104175.

7. Chen, J.; Tong, J.; Rui, Y.; Cui, Y.; Pu, Y.; Du, J.; Apel, D.B. Step-path failure mechanism and stability analysis of water-bearing rock slopes based on particle flow simulation. *Theor. Appl. Fract. Mech.* **2024**, *131*, 104370.
8. Fan, X.; Xu, Q.; Scaringi, G.; Zheng, G.; Huang, R.; Dai, L.; Ju, Y. The "long" runout rock avalanche in Pusa, China, on august 28, 2017: A preliminary report. *Landslides* **2019**, *16*, 139–154. [CrossRef]
9. Esterhuizen, G.S.; Tyrna, P.L.; Murphy, M.M. A case study of the collapse of slender pillars affected by through-going discontinuities at a limestone mine in Pennsylvania. *Rock Mech. Rock Eng.* **2019**, *52*, 4941–4952.
10. Reed, M.; Steve, K. Peripheral gully and landslide erosion on an extreme anthropogenic landscape produced by mountaintop removal coal mining. *Earth Surf. Process. Landf.* **2020**, *45*, 2078–2090.
11. Luo, R.; Li, G.Y.; Chen, L.; Yang, Q.Y.; Zang, C.W.; Cao, W.Z. Ground subsidence induced by pillar deterioration in abandoned mine districts. *J. Cent. South Univ.* **2020**, *27*, 2160–2172.
12. Yang, C.; Shi, W.; Peng, X.; Zhang, S.; Wang, X. Numerical simulation of layered anti-inclined mining slopes based on different free face characteristics. *Bull. Eng. Geol. Environ.* **2022**, *81*, 359.
13. Li, Z.F.; Zhang, Y.J.; Huang, J.X.; Luo, Z.M. Stability analysis of karst subgrade roof considering spatial form of the Karst cave. *Highw. Automot. Appl.* **2023**, *216*, 66–72.
14. Salmi, E.; Nazem, M.; Karakus, M. Numerical analysis of a large landslide induced by coal mining subsidence. *Eng. Geol.* **2017**, *217*, 141–152.
15. Arca, D.; Kutoğlu, H.; Becek, K. Landslide susceptibility mapping in an area of underground mining using the multicriteria decision analysis method. *Environ. Monit. Assess.* **2018**, *190*, 725.
16. Cui, F.; Xiong, C.; Wu, Q.; Li, B.; Luo, W.; Pei, Y.Q. Dynamic mechanism triggering an underground-mining induced landslide in karst mountains, Southwest China. *Bull. Eng. Geol. Environ.* **2023**, *82*, 449.
17. Yang, D.; Qiu, H.; Ma, S.; Liu, Z.; Du, C.; Zhu, Y.; Cao, M. Slow surface subsidence and its impact on shallow loess landslides in a coal mining area. *Catena* **2022**, *209*, 0341–8162.
18. Lai, Q.; Zhao, J.; Shi, B.; Liu, H.; Ji, L.; Li, Q.; Huang, R. Deformation evolution of landslides induced by coal mining in mountainous areas case study of the Madaling landslide, Guizhou, China. *Landslides* **2023**, *20*, 2003–2016.
19. Liu, F.; Yang, Z.; Deng, W.; Yang, T.; Zhou, J.; Yu, Q.; Mao, Y. Rock landslide early warning system combining slope stability analysis, two-stage monitoring, and case-based reasoning a case study. *Bull. Eng. Geol. Environ.* **2021**, *80*, 8433–8451.
20. Zhong, J.; Mao, Z.; Ni, W.; Zhang, J.; Liu, G.; Zhang, J.; Geng, M. Analysis of formation mechanism of slightly inclined bedding mudstone landslide in coal mining subsidence area based on finite–discrete element method. *Mathematics* **2022**, *10*, 3995. [CrossRef]
21. Dhahri, F.; Benassi, R.; Mhamdi, A.; Zeyeni, K.; Boukadi, N. Structural and geomorphological controls of the present-day landslide in the Moulares phosphate mines (western-central Tunisia). *Bull. Eng. Geol. Environ.* **2016**, *75*, 1459–1468. [CrossRef]
22. Rui, Y.; Chen, J.; Chen, J.; Qiu, J.; Zhou, Z.; Wang, W.; Fan, J. A robust triaxial localization method of AE source using refraction path. *Int. J. Min. Sci. Technol.* **2024**, *34*, 521–530. [CrossRef]
23. Li, H.J.; Dong, J.H.; Zhu, Y.Q.; Zou, Y.X.; Ding, H. Characteristics and genesis mechanism of Jianshanying landslide in Faer coal mine, Guizhou province. *Sci. Technol. Eng.* **2019**, *19*, 345–351.
24. Zhao, Q.; Yang, Z.; Jiang, Y.; Liu, X.; Cui, F.; Li, B. Discrete element analysis of deformation features of slope controlled by Karst fissures under the mining effect: A case study of Pusa landslide, China. *Geomat. Nat. Hazards Risk* **2023**, *14*, 1–35.
25. Stephen, H.; Valery, V.; Richard, G.; Philippe, C. Behavior in mixed-mode of desiccation cracks on a clayey rock front gallery. *Int. J. Rock Mech. Min. Sci.* **2022**, *154*, 105104.
26. Chen, L.; Zhou, Z.; Zang, C.; Zeng, L.; Zhao, Y. Failure pattern of large-scale goaf collapse and a controlled roof caving method used in gypsum mine. *Geomech. Eng.* **2019**, *18*, 449–457.
27. Zhu, W.; Chen, L.; Zhou, Z.; Shen, B.; Xu, Y. Failure propagation of pillars and roof in a room and pillar mine induced by longwall mining in the lower seam. *Rock Mech. Rock Eng.* **2019**, *52*, 1193–1209.
28. Zhao, Y.; Zhao, G.; Zhou, J.; Ma, J.; Cai, X. Failure mechanism analysis of rock in particle discrete element method simulation based on moment tensors. *Comput. Geotech.* **2021**, *136*, 104215.
29. Zhong, H.; Liang, C.; Chen, L.; Gao, S. Characteristics of large deformation and prevention methods for shallow buried large span tunnels. *J. Transp. Sci. Eng.* **2024**, *40*, 71–78.
30. Potyondya, D.; Cundall, P. A bonded-particle model for rock. *Int. J. Rock Mech. Min. Sci.* **2004**, *41*, 1329–1364. [CrossRef]
31. Zhou, Z.; Chen, L.; Zhao, Y.; Zhao, T.; Cai, X.; Du, X. Experimental and numerical investigation on the bearing and failure mechanism of multiple pillars under overburden. *Rock Mech. Rock Eng.* **2017**, *50*, 995–1010. [CrossRef]

Disclaimer/Publisher's Note: The statements, opinions and data contained in all publications are solely those of the individual author(s) and contributor(s) and not of MDPI and/or the editor(s). MDPI and/or the editor(s) disclaim responsibility for any injury to people or property resulting from any ideas, methods, instructions or products referred to in the content.